The FEBS Journal

FEBS PRESS science publishing by scientists

Creation of RANKL mutants with low affinity for decoy receptor OPG and their potential anti-fibrosis activity

Yizhou Wang, Timo Michiels, Rita Setroikromo, Ronald van Merkerk, Robbert H. Cool and Wim J. Quax

Department of Chemical and Pharmaceutical Biology, Groningen Research Institute of Pharmacy, University of Groningen, The Netherlands

Keywords
fibrosis; liver; lung; OPG; RANK

Correspondence
W. J. Quax, Department of Chemical and Pharmaceutical Biology, Groningen Research Institute of Pharmacy, University of Groningen, A. Deusinglaan 1, Groningen 9713 AV, The Netherlands
Tel: +31 50 363 2558
E-mail: w.j.quax@rug.nl

(Received 17 December 2018, revised 11 April 2019, accepted 10 May 2019)

doi:10.1111/febs.14925

Fibrosis is characterized by the progressive alteration of the tissue structure due to the excessive production of extracellular matrix (ECM). The signaling system encompassing Receptor Activator of Nuclear factor NF-κB Ligand (RANKL)/RANK/Osteoprotegerin (OPG) was discovered to play an important role in the regulation of ECM formation and degradation in bone tissue. However, whether and how this signaling pathway plays a role in liver or pulmonary ECM degradation is unclear up to now. Interestingly, increased decoy receptor OPG levels are found in fibrotic tissues. We hypothesize that RANKL can stimulate RANK on macrophages and initiate the process of ECM degradation. This process may be inhibited by highly expressed OPG in fibrotic conditions. In this case, RANKL mutants that can bind to RANK without binding to OPG might become promising therapeutic candidates. In this study, we built a structure-based library containing 44 RANKL mutants and found that the Q236 residue of RANKL is important for OPG binding. We show that RANKL_Q236D can activate RAW cells to initiate the process of ECM degradation and is able to escape from the obstruction by exogenous OPG. We propose that the generation of RANKL mutants with reduced affinity for OPG is a promising strategy for the exploration of new therapeutics against fibrosis.

Introduction

The cytokine system consisting of receptor activator of nuclear factor NF-κB ligand (RANKL), RANK and Osteoprotegerin (OPG), plays a key role in bone homeostasis by controlling the balance between bone producing and bone resorbing activity [1]. RANKL is expressed on osteoblasts and its receptor RANK is expressed on osteoclast precursor cells [2]. As a member of the tumor necrosis factor (TNF) superfamily, RANKL is a type II transmembrane protein with a C-terminal extracellular region [3–5]. The binding between RANKL and RANK on osteoclast precursors induces the expression of osteoclast-specific genes, including tartrate-resistant acid phosphatase (TRAP), cathepsin K, matrix metallopeptidase 9 (MMP9), which will further trigger osteoclast maturation and bone extracellular matrix (ECM) degradation [6,7]. Osteoprotegerin (OPG) is produced by osteoblasts and acts as a natural decoy receptor for RANKL thereby inhibiting osteoclast activation and bone ECM degradation [8]. Imbalances in the RANK/RANKL/OPG pathway can differently regulate the orientation of bone remodeling to either bone formation or

Abbreviations
CPD, Computational Protein Design; ECM, extracellular matrix; MMP, matrix metallopeptidase; mRANKL, murine RANK ligand; mRANK, murine RANK; OPG, osteoprotegerin; pNPP, paranitrophenylphosphate; RANKL, receptor activator of nuclear factor-κB ligand; RANK, receptor activator of nuclear factor-κB; SPR, surface plasmon resonance; TGF-β, transforming growth factor beta; TNF, tumor necrosis factor; TRAIL, tumor necrosis factor-related apoptosis-inducing ligand; TRAP, tartrate-resistant acid phosphatase.

resorption, therefore leading to diseases such as osteoporosis with a high RANKL/OPG ratio and osteopetrosis with a low RANKL/OPG ratio [9–12].

Fibrosis is a chronic disease characterized by excessive accumulation of ECM and destruction of tissue structure in response to injury [13,14]. With a high mortality rate, fibrotic diseases cause more than 800 000 deaths every year worldwide [14]. However, there is no effective therapy to reverse chronic fibrosis currently. Taking pulmonary fibrosis as an example, lung transplantation is the only effective way to treat lung fibrosis at present [13,15,16]. Fibroblasts and myofibroblasts are the most important cells involved in the production of ECM [17]. Macrophages, which are also abundantly present in fibrotic tissue, however, have been shown to possess both profibrotic and antifibrotic properties leading to different phenotypes [18,19]. They have been identified to secrete inflammatory and growth factors such as transforming growth factor beta (TGF-β), IL-13 and TNF, which promote the fibrotic process [14,15]. On the other hand, macrophages in fibrotic tissues also possess antifibrotic properties by producing secreted matrix metalloproteinases (MMPs) and cathepsins that degrade fibrotic ECM [20]. However, how antifibrotic macrophages are activated and induced to degrade ECM still remains to be understood.

Interestingly, many tissue macrophages express RANK, and through RANKL stimulation, proteases are released which can degrade ECM [20]. In bone, osteoclasts are derived from macrophage/monocyte and can produce MMPs and other proteolytic enzymes to degrade bone ECM [21,22]. In fibrotic tissue, the stimulation of the RANKL/RANK axis may also be a possible way to activate antifibrotic macrophages and reverse fibrosis [20]. Notably, OPG, as a decoy receptor of RANKL, was shown to be an inducer of fibrogenesis to promote vascular fibrosis in vascular smooth muscle cells [23]. High expression of OPG was found to be related to the formation of fibrous tissues in diseases like liver, vasculature, and cystic fibrosis [24,25], suggesting that OPG may be important in the fibrosis process, which is a further support for the a role of the RANKL/RANK/OPG axis in fibrosis.

In the present research, we hypothesized that RANKL could stimulate RANK on macrophages and initiate the process of ECM degradation. This process may be inhibited by the decoy activity of highly expressed OPG in fibrotic conditions. As a consequence, RANKL mutants that can bind to RANK without binding to OPG are becoming promising agonists to stimulate RANK on macrophages and reduce ECM without being hampered by high OPG production. Therefore, in this research, through comparing the 3D structures of murine RANKL–RANK and RANKL–OPG, we have built a structure-based RANKL mutants library containing 44 RANKL mutants. Our results show that RANKL_Q236D is very effective in activating murine RAW 264.7 macrophage cells and to escape from the obstruction by exogenous OPG. The generation of RANKL mutants with reduced binding to OPG is a promising strategy for the exploration of new therapeutics against fibrosis.

Results

RANKL–RANK- and RANKL–OPG-binding interface analysis and structure-based design of the mutants

The available 3D structures of murine RANKL–RANK and RANKL–OPG complexes (Protein Data Bank accession codes 4GIQ and 4E4D) were used to perform binding simulations. As shown in Fig. 1A, via analysis of all interactions—including hydrogen bonds, electrostatic, and hydrophobic properties—between RANKL–RANK and RANKL–OPG, all residues of RANKL that show interactions with one or both receptors were identified. These residues are marked from light to dark purple according to the number of interactions they were involved in (Fig. 1A). RANKL_Q236, I248, and K256 were selected for mutation because they show interactions with OPG, but not RANK (Fig. 1B,C and Table 1). Therefore, it is supposed that these can change the binding of RANKL to OPG without influencing the binding of RANKL to RANK. In addition, RANKL_R190, R222, H252, and E268 were selected, because these four residues show more interactions with OPG than RANK (Fig. 1B,C and Table 1), suggesting that the effect on RANKL–RANK interactions by replacing them might be minimal.

In silico mutagenesis at positions Q236, I248, K256, R190, R222, H252, and E268 was performed to estimate differences between RANKL mutants and RANKL_WT in $\Delta\Delta G_i$ binding to receptors (Fig. 2). A more negative $\Delta\Delta G_i$ value indicates a predicted increase in receptor binding energy, and vice versa. Based on the outcome, we decided to select and construct a subset of RANKL mutants. Two residues, RANKL_Q236 and K256, were subjected to full saturation mutagenesis, because for these two positions all the other 19 amino acids were predicted to give a decrease in affinity for OPG (Fig. 2A,B). Other single substitutions of RANKL_I248W, H252W, H252L, H252R, E268D, and E268N were selected on the basis

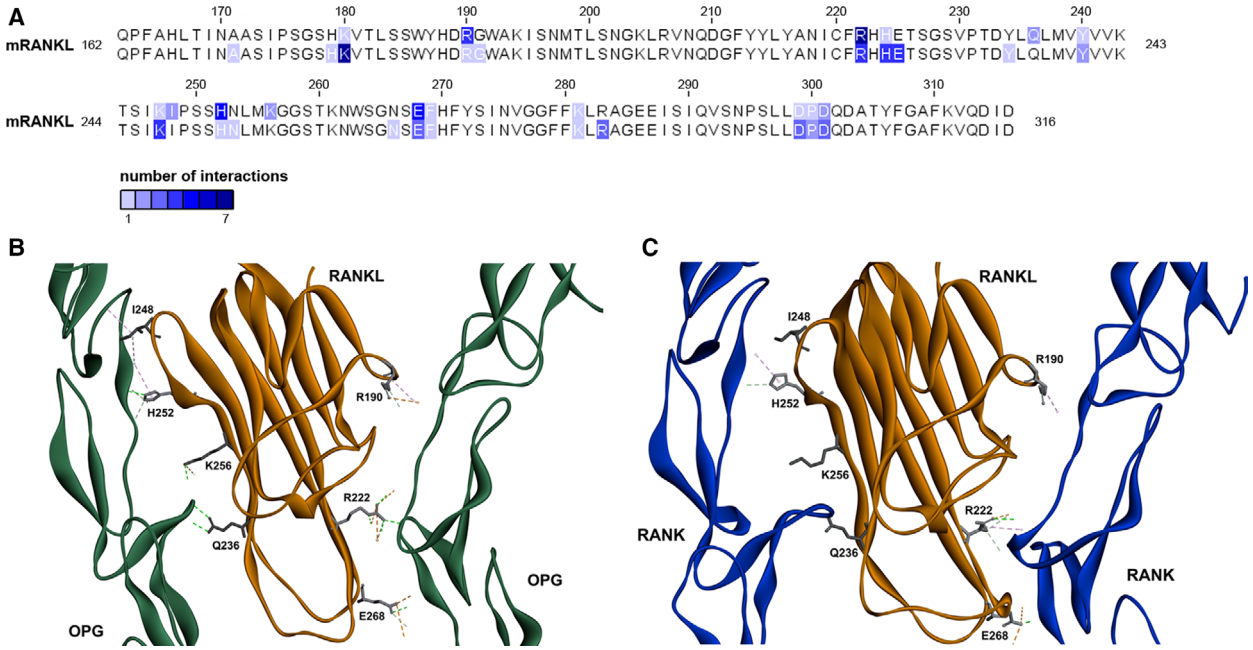

Fig. 1. Structural comparison of RANKL/OPG and RANKL/RANK made using DISCOVERY STUDIO 4.5. (A) Structural comparison between RANKL/OPG (upper sequence) and RANKL/RANK (bottom sequence). The color represents the residue shows interaction with receptor and the range of color form light blue to dark blue indicates the number of interactions. (B, C) Detailed view of selected RANKL residues (R190, R222, I248, Q236, H252, K256, and E268) and their interactions with OPG and RANK.

of their predicted lowered affinity for OPG or their large difference of predicted affinities for OPG and RANK. In total 44 variants were proposed.

Prescreen of RANKL mutants with reduced binding to OPG

After construction, expression, and purification using cation exchange chromatography, 28 out of these 44 variants were obtained successfully. Most RANKL_K256 variants, however, were produced in inclusion bodies. On hindsight, this can be explained by the role this residue plays in RANKL trimerization, which forms a polar interaction with D303 within the neighbor monomer [4]. Changing this lysine into any other amino acid might prevent the formation of the RANKL trimer. The double mutant RANKL_K256D/D303K could not rescue the folding of the protein as well. Apparently, no changes are tolerated at this position and therefore the 256 variants were not used for further investigations. To assess the binding of RANKL variants to immobilized RANK-Fc and OPG-Fc, an ELISA assay was performed (Fig. 3). Several RANKL_236 variants RANKL_Q236N, Q236S, Q236D, Q236H, Q236P, and Q236A showed an increase in the binding ratio of RANK versus OPG. Compared to RANKL_WT, they all showed higher binding to RANK and 40–60% lower binding to OPG. Especially, RANKL_Q236D was of interest as it displayed a low binding to OPG, which is at 25% of that of RANKL_WT. Variant RANKL_Q236K was also selected for further analysis as it showed a large decrease in binding to OPG with, however, a concomitant lower ELISA signal in binding to RANK.

Receptor binding affinity of RANKL variants as determined by SPR

Seven promising candidates, which maintained the binding to RANK-Fc and showed decreased binding to OPG-Fc were selected following the ELISA data. These variants were purified to homogeneity as described before [10]. Affinities of the purified RANKL variants to RANK and OPG receptors were determined using surface plasmon resonance (SPR). By using the CM4 sensorchip, with a low density of receptor, we were able to achieve complexes of RANKL–RANK and RANKL–OPG in the form of mixtures of trimer–monomer and trimer–dimer [26]. All the data were fitted with a 1 : 1 Langmuir fitting model and the kinetic parameters were calculated and shown in Table 2. All these seven RANKL mutants showed much lower affinities to OPG-Fc with the best one RANKL_Q236D showing around a three-time

Table 1. Interaction analysis between RANKL–OPG and RANKL–RANK complexes.

	RANKL–OPG		RANKL–RANK	
	Interaction	Category	Interaction	Category
K256	RANKL:K256:NZ–OPG1:E95:OE2	Electrostatic		
	RANKL:K256:HZ2–OPG1:E95:OE1	Hydrogen bond		
Q236	RANKL:Q236:HE21–OPG1:E93:O	Hydrogen bond		
	OPG1:E95:HN–RANKL:Q236:OE1	Hydrogen bond		
I248	OPG1:V60–RANKL:I248	Hydrophobic		
	OPG1:H54–RANKL:I248	Hydrophobic		
R190	RANKL:R190:HD1–OPG2:Y61:OH	Hydrogen bond	RANKL:R190–RANK2:L59	Hydrophobic
	RANKL:R190:HD2–OPG2:Y61:OH	Hydrogen bond		
	RANKL:R190:NH1–OPG2:H47	Electrostatic		
	OPG2:Y61–RANKL:R190	Hydrophobic		
H252	RANKL:H252:HD1–OPG1:S63:OG	Hydrogen bond	RANKL:H252:HE1–RANK1:Y47:OH	Hydrogen bond
	OPG1:Y49:HH–RANKL:H252:NE2	Hydrogen bond	RANKL:H252–RANK1:L58	Hydrophobic
	RANKL:H252:HE1–OPG1:Y61:O	Hydrogen bond		
	RANKL:H252:HE1–OPG1:S63:O	Hydrogen bond		
	RANKL:H252–OPG1:V60	Hydrophobic		
E268	OPG2:R90:HH12–RANKL:E268:OE2	Hydrogen bond; Electrostatic	RANK2:R99:NH1–RANKL:E268:OE2	Electrostatic
	OPG2:K99:NZ–RANKL:E268:OE2	Electrostatic	RANK2:R100:HN–RANKL:E268:OE2	Hydrogen bond
	OPG2:R90:HH21–RANKL:E268:OE1	Hydrogen bond	RANK2:R100:NH1–RANKL:E268:OE2	Electrostatic
	OPG2:K99:HE1–RANKL:E268:OE1	Hydrogen bond		
	OPG2:K99:HE2–RANKL:E268:OE1	Hydrogen bond		
R222	RANKL:R222:NH1–OPG2:E68:OE2	Electrostatic	RANKL:R222:HH11–RANK2:D64:OD2	Hydrogen bond; Electrostatic
	RANKL:R222:NH1–OPG2:E95:OE2	Electrostatic	RANKL:R222:HD1–RANK2:D64:OD2	Hydrogen bond
	RANKL:R222:HE–OPG2:E68:OE2	Hydrogen bond	RANKL:R222:HD2–RANK2:G66:O	Hydrogen bond
	RANKL:R222:HH12–OPG2:E95:OE1	Hydrogen bond	RANKL:R222–RANK2:K67	Hydrophobic
	RANKL:R222:HH21–OPG2:E68:OE1	Hydrogen bond		
	RANKL:R222:HH22–OPG2:E95:O	Hydrogen bond		
	RANKL:R222:NH1–OPG2:F96	Electrostatic		

decrease in the association rate constant (k_a) and a 10-fold increase in the dissociation rate constant (k_d), which taken together is a 30-time decrease in affinity to OPG-Fc (Fig. 4). Importantly, this same mutant maintained its affinity to RANK-Fc. RANKL_Q236K, however, has a much lowered affinity to RANK-Fc as suggested by its lower ELISA signal. RANKL mutants Q236N, Q236S, Q236H, Q236P, and Q236A, all showed affinities to RANK-Fc that are in the same range or slightly lower than RANK_WT, between 50% and 100%, which is mainly due to higher dissociation rates. Taken together, these results are consistent with the previous prescreen ELISA result and they further confirm that the RANKL_Q236 residue indeed plays an important role in RANKL–OPG binding with RANKL_Q236D showing the most promising properties.

Effect of RANKL variants on ECM degradation enzymes expression in RAW 264.7 cells

In bone regulation process, the binding between RANKL and the RANK on osteoclast precursors will induce the expression of osteoclast-specific genes, such as TRAP and MMP9, which will stimulate osteoclast maturation and bone ECM degradation [22]. In fibrosis, MMPs have been shown to be responsible for collagen degradation and ECM breakdown, which is actually beneficial for fibrosis recovery [14,19]. Furthermore, MMP9 is particularly expressed in

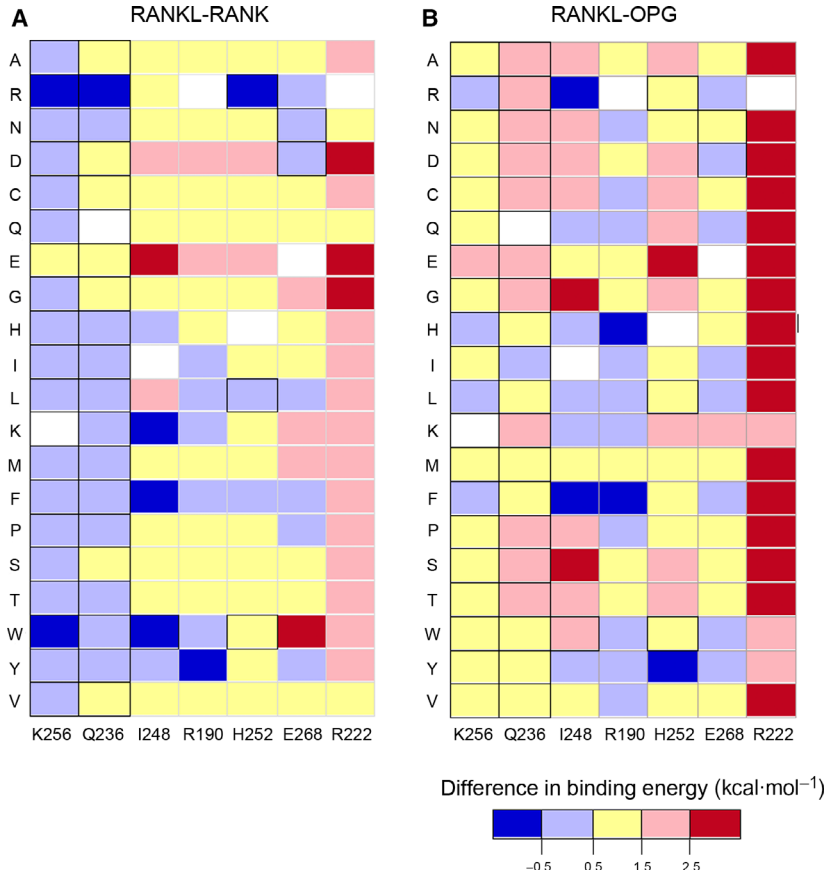

Fig. 2. Heatmap of the binding energy predictions for RANKL_mutants. Predicted differences in binding energy ($\Delta\Delta G_i$) of RANKL_K256, Q236, I248, R190, H252, E268, and R222 variants binding to RANK (A) and OPG (B) when compared with RANKL_WT are shown in the heatmap respectively. A negative $\Delta\Delta G_i$ value indicates an improvement in receptor binding, whereas a positive $\Delta\Delta G_i$ value indicates a decrease in receptor binding.

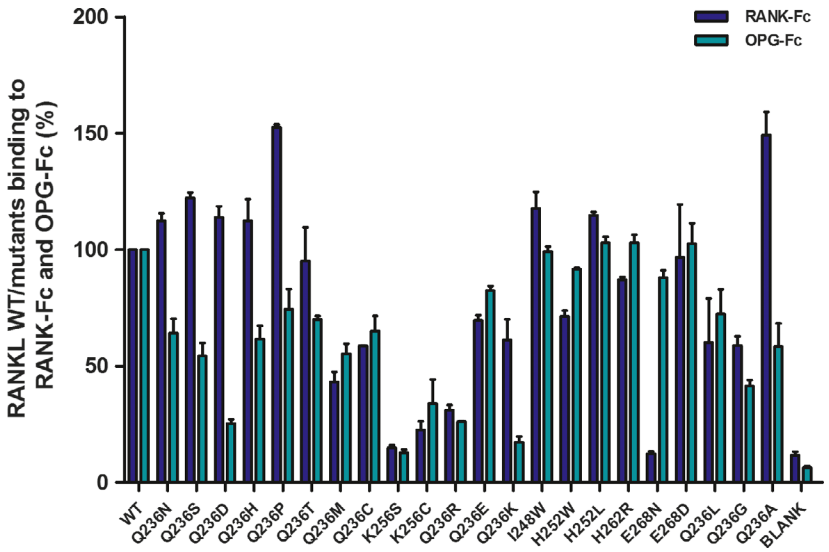

Fig. 3. Comparison of the relative bindings of RANKL mutants towards mOPG-Fc and RANK-Fc, as determined by ELISA. Receptor binding to mOPG-Fc and RANK-Fc was performed in duplo and calculated relative to the response of RANKL_WT (100%) at 0.5 nM.

macrophages within lung and liver [20]. Therefore, we chose a monocyte-derived RAW 264.7 macrophage as a cell model to detect the biological effects caused by RANKL variants. Real-time quantitative PCR was performed to detect the TRAP and MMP9 gene expressions in the presence of RANKL variants with or without exogenous OPG. As shown in Fig. 5, RANKL_WT (50 ng·mL^{-1}) stimulation could significantly induce the expressions of MMP9 and TRAP, which was totally blocked by adding exogenous mOPG-Fc at the concentration of 400 ng·mL^{-1}. Interestingly, the addition of mOPG-Fc did have much less

Table 2. Binding kinetics of the RANKL variants and RANKL_WT to mRANK-Fc and mOPG-Fc by surface plasmon resonance.

	OPG-Fc			RANK-Fc		
Protein	$k_a \times 10^{-7}$ ($M^{-1}\cdot s^{-1}$)	$k_d \times 10^4$ (s^{-1})	K_D (pM)	$k_a \times 10^{-6}$ ($M^{-1}\cdot s^{-1}$)	$k_d \times 10^4$ (s^{-1})	K_D (pM)
RANKL_WT	1.8 ± 0.7	0.7 ± 0.1	4.3 ± 1.6	8.4 ± 0.6	1.0 ± 0.1	11.9 ± 1.5
RANKL_Q236N	1.5 ± 0.2	3.1 ± 0.9	20.7 ± 3.7	7.9 ± 0.9	1.7 ± 0.3	22.1 ± 2.9
RANKL_Q236H	1.3 ± 0.2	2.2 ± 0.5	16.6 ± 1.6	6.7 ± 0.0	1.3 ± 0.2	18.7 ± 2.8
RANKL_Q236S	1.4 ± 0.2	3.1 ± 0.4	23.3 ± 4.5	7.0 ± 0.6	1.8 ± 0.5	24.9 ± 5.1
RANKL_Q236D	0.6 ± 0.1	7.0 ± 1.0	112.3 ± 24.4	6.4 ± 0.8	0.9 ± 0.2	15.0 ± 3.2
RANKL_Q236A	1.6 ± 0.3	3.3 ± 0.4	20.5 ± 2.2	8.9 ± 2.0	1.8 ± 0.3	21.5 ± 6.6
RANKL_Q236K	1.1 ± 0.5	14.6 ± 2.7	142.7 ± 44.6	8.0 ± 1.3	9.5 ± 0.8	119.3 ± 10.5
RANKL_Q236P	1.1 ± 0.3	2.2 ± 0.3	21.3 ± 8.2	6.1 ± 0.5	1.2 ± 0.4	19.8 ± 6.0

influence on the activation by RANKL variants as compared to that by RANKL_WT. Activation by RANKL_Q236D was not inhibited at all by the presence of mOPG-Fc indicating that this variant is capable of restoring MMP9 activity in fibrotic tissues.

Effect of RANKL variants on RANKL induced osteoclastogenesis in RAW 264.7 cells

To further confirm the role of RANKL variants, we next tested their effects on osteoclastogenesis in the presence of mOPG-Fc. RAW 264.7 cells were treated with RANKL_WT and variants with or without the presence of mOPG-Fc. After 4 days, the cells were measured for TRAP activity and osteoclasts formation, respectively. As shown in Fig. 6A,B, RANKL_WT could significantly induce both TRAP activation and osteoclast formation. This activation was totally blocked by the addition of mOPG-Fc. Treatments with RANKL variants Q236N, Q236S, Q236H, Q236P, and Q236A could induce TRAP activity at a level comparable with RANKL_WT (Fig. 6A). Interestingly, these RANKL variants exhibited less inhibition by the addition of OPG-Fc and they were capable to retain from 50% to 80% of TRAP activity in the presence of OPG-Fc. RANKL_Q236K could no longer induce TRAP activity because of its lower affinity to RANK. Fascinatingly, RANKL_Q236D could almost completely escape from the inhibition by OPG and kept approximately 95% of TRAP activity. Consistently, in the osteoclast formation assay (Fig. 6B), RANKL_Q236N, Q236S, Q236H, Q236P, and Q236A could only induce 18% to 54% of osteoclast formation in the presence of 400 $ng\cdot mL^{-1}$ of mOPG-Fc, while RANKL_Q236D still showed complete activation at the same concentration of mOPG-Fc. Microscope photographs of osteoclasts from treatments with RANKL_WT (50 $ng\cdot mL^{-1}$) and RANKL_Q236D (50 $ng\cdot mL^{-1}$), both in the presence and absence of mOPG-Fc are shown in Fig. 6C. Both single treatments with RANKL_WT and RANKL_Q236D instigated a massive osteoclast formation. The addition of 400 $ng\cdot mL^{-1}$ of mOPG-Fc could completely block osteoclast formation caused by RANKL_WT, but showed no influence on that caused by RANKL_Q236D.

Discussion

The RANKL/RANK/OPG system was discovered decades ago and is most prominently known for its role in regulating bone density [27,28]. Nowadays this system is known to be more versatile and is also thought to be involved in the process of fibrosis [20,29,30]. High expression of OPG was found to be related to fibrosis diseases like liver, vascular, and cystic fibrosis, suggesting an important role of OPG in fibrosis [23–25]. Recently, it was suggested that inefficient RANKL stimulation occurs in lung tissues of human and mice with pulmonary fibrosis [20] supporting the idea that the decoy activity of OPG plays a role in fibrosis. In this study, we hypothesized that RANKL could stimulate RANK on macrophages and initiate the process of ECM degradation, which may be inhibited by high OPG levels in fibrotic conditions. Therefore, RANKL mutants, which can bind to RANK without binding to OPG, are becoming of interest to solely stimulate RANK on macrophages and reduce ECM without binding to OPG present in fibrotic tissue. Notably, OPG also acts as the decoy receptor of tumor necrosis factor-related apoptosis-inducing ligand (TRAIL), the other member of the TNF superfamily, and recently a TRAIL variant DHER lacking binding to OPG, was developed [31,32], which indicates the possibility of making RANKL variants as well.

The available 3D structures of murine RANKL–RANK and RANKL–OPG complexes (Protein Data Bank accession codes 4GIQ and 4E4D) were used as the starting point for inspecting the binding surface. Several residues of mRANKL, Q236, I248, K256,

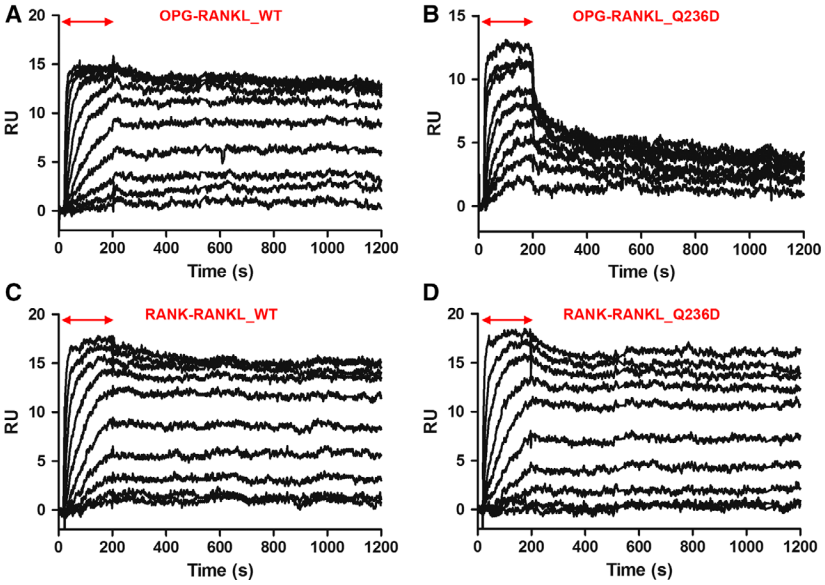

Fig. 4. Typical SPR sensorgrams obtained for binding between RANK-Fc/OPG-Fc and RANKL_WT/RANKL_Q236D. Depicted are the binding between (A) OPG-Fc and RANKL_WT, (B) OPG-Fc and RANKL_Q236D, (C) RANK-Fc and RANKL_WT, and (D) RANK-Fc and RANKL_Q236D. Injection of RANKL is marked with a double-headed arrow. After injection, the dissociation was followed for 1000 s.

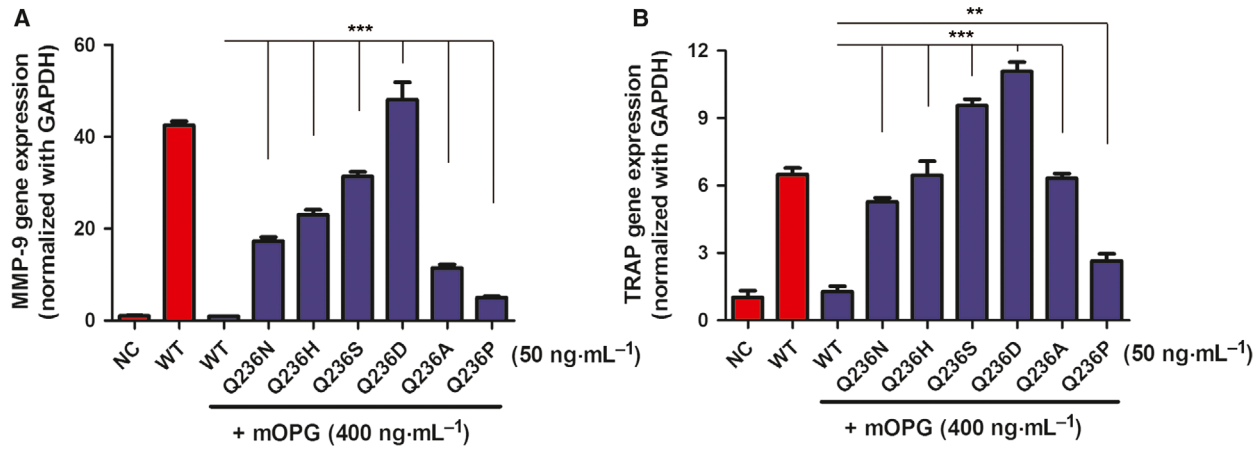

Fig. 5. mRNA levels of different ECM-degrading enzymes, (A) MMP 9 and (B) TRAP, after treatment with RANKL_WT and mutants, determined by real-time quantitative PCR. Significance was calculated using a Student's *t*-test compared to cells treated with RANKL_WT (50 ng·mL^{-1}) plus mOPG-Fc (400 ng·mL^{-1}): (**) is $P < 0.01$ and (***) is $P < 0.0001$. The error bars reflect the standard deviation of three independent experiments.

R190, R222, H252, and E268, stand out from the analysis as they show more interactions with OPG than RANK. *In silico* calculation of differences in $\Delta\Delta G_i$ binding to receptors helped us to further reduce the range of selection. The selected residues are located in the C-D loop, D-E loop, E strand, and F strand of RANKL, respectively. This is consistent with a previous analysis by Nelson *et al.* [33] that the contacts made by OPG are limited to the E strand and D-E loop region of RANKL. Upon expression, unfortunately, RANKL K256 variants were not being properly folded and insoluble aggregates were formed. Lam *et al.* [4] discussed that position 256 is involved in the trimeric interface of RANKL and it forms an ionic interaction with D303 of the neighboring monomer. Our attempt to restore the ionic bond by making the reciprocal double mutation K256D/D303K could not rescue the folding of the protein. More refined studies on position mRANKL_K256 might still be of interest as Luan *et al.* [34] suggested that hRANKL_K257, which is the equivalent to mRANKL_K256, interacts with the E95 residue of hOPG-CRD.

Computational Protein Design (CPD) methods have been successfully used for analyzing and modifying protein–protein interactions by us [32,35]. Compared to traditionally directed evolution, which produces and evaluates mutations at many positions, CPD can guide us directly to focus on certain key amino acids in a

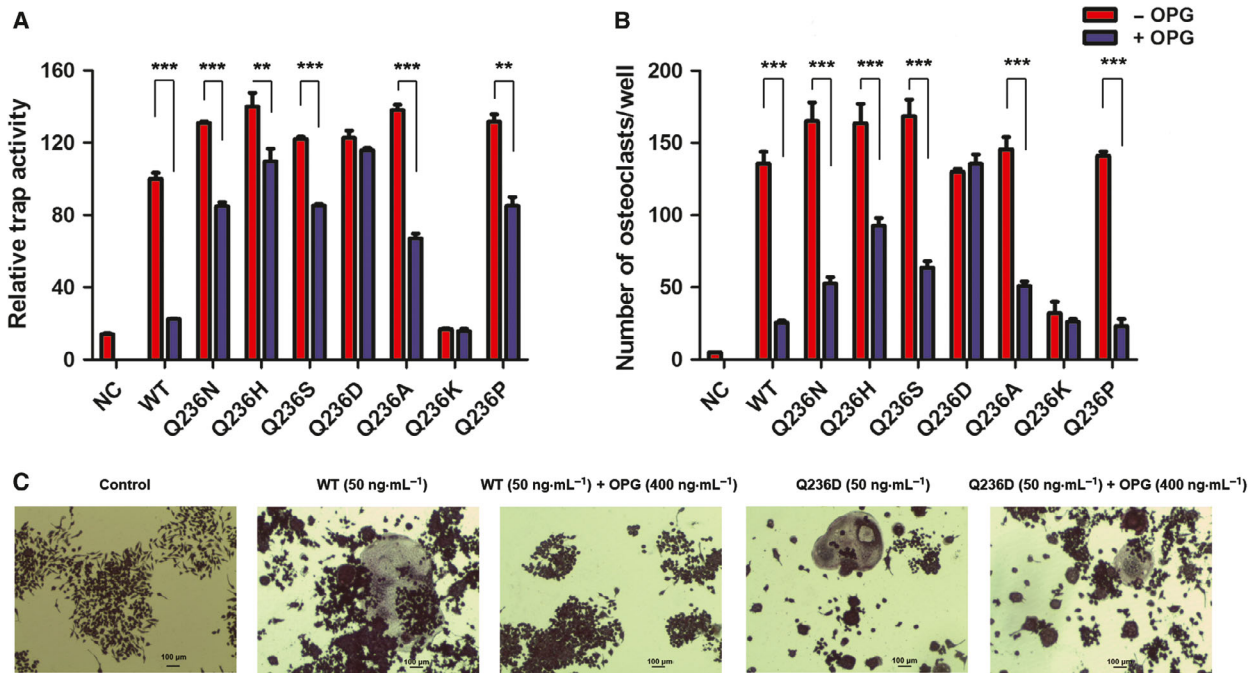

Fig. 6. Effect of RANKL variants on RANKL induced osteoclastogenesis in RAW 264.7 cells. (A) TRAP activity and (B) relative number of osteoclasts obtained after treatment of murine RAW 264.7 cells with RANKL variants (50 ng·mL^{-1}) and RANKL_WT (50 ng·mL^{-1}) with or without mOPG-Fc (400 ng·mL^{-1}). (C) Microscope images of RAW 264.7 cells treated with RANKL_WT and RANKL_Q236D with or without mOPG-Fc. Scale 100 μm. Significance was calculated using a Student's *t*-test: (**) is $P < 0.01$ and (***) is $P < 0.0001$. The error bars reflect the standard deviation of three independent experiments.

much shorter time. Therefore, the combination of CPD and focused mutagenesis and screening is efficient as exemplified by the mutant Q236D. However, there are limitations in the predictions given by CPD and the factual results can differ from predictions as exemplified by the mutants of residue K256.

Receptor binding experiments using prescreen ELISA and SPR confirmed the predictions from the design that residue Q236 is one of the most important residues for OPG binding. On the basis of the ELISA results, we purified RANKL_Q236N, Q236S, Q236H, Q236D, Q236P, Q236K, and Q236A and using SPR all were shown to have decreased affinity for OPG in accordance with the *in silico* predictions. All of them, except Q236K, have affinities for RANK comparable to RANKL_WT (Table 2). RANKL_Q236D is the best among them to have approximately a 30-time decrease in affinity to OPG-Fc. In line with these results, structural analysis of this mutation (Fig. 7A,B) shows that the single substitution at 236 position from glutamine to aspartate reduces the length of the side chain. Therefore, the distance from RANKL 236 to OPG E93 and E95 becomes larger, and two hydrogen bonds might disappear that are normally present between RANKL Q236 and OPG residues E93 and E95. On the other hand, the negatively charged aspartate on position 236 may have repulsion to the negatively charged E93 and E95 residues on the OPG surface. Interestingly, Warren *et al.* [36] previously selected RANKL_Q236H from an error-prone PCR library using yeast display to have a decrease in binding to OPG. Here, we used saturation mutagenesis and among others also selected RANKL_Q236H to show a lower affinity to OPG. Thanks to the saturation mutagenesis, we selected a superior variant, RANKL_Q236D, which has a 6.8-time decrease in affinity to OPG compared to RANKL_Q236H. This novel variant shows superior properties to initiate the process of ECM degradation in fibrotic tissue, which is typified by an excess of OPG [20,24]. In the further development of this variant towards a therapeutic drug it should be noted that the RANKL/RANK/OPG pathway also plays an important role in bone remodeling. Therefore, a tissue-specific delivery of RANKL_Q236D is needed to achieve targeting of fibrotic organs directly without influencing the bone remodeling. As fibrosis can occur in many different organs showing a common pathogenic pathway and the presence of matrix proteins is highly similar, it is suggested that promoting ECM degradation could be a common way for organ repair [37]. Drug delivery systems that can target these different organs will be

the topic of our future research. As it is crucial and essential to identify alternative therapeutic strategies for fibrosis treatment [16,38], we think our approach is worthwhile pursuing.

In conclusion, we have built a structure-based RANKL mutant library containing 44 RANKL mutants and the Q236 residue of RANKL is of importance for OPG binding. RANKL_Q236D was found to maintain activating RAW 264.7 cells and to escape from the obstruction by exogenous OPG. Notably, the antifibrotic effect of RANKL_Q236D is deserved to be evaluated *in vivo*. In our study, the importance of the RANKL Q236 residue in RANKL–OPG binding and the discovery of RANKL_Q236D variant form a starting point for the exploration of new therapeutics against fibrosis.

Experimental procedures

In silico calculation

Binding simulations were performed using the available 3D structures of murine RANKL–RANK and RANKL–OPG complexes (Protein Data Bank accession codes 4GIQ and 4E4D). BIOVIA DISCOVERY STUDIO 4.5 (Accelrys, CA, USA) was used to perform all the calculations and predictions. Briefly, homotrimer structures of RANKL–RANK and RANKL–OPG were prepared and minimized based on CHARMm force field as previously described [10]. Generalized Born with molecular volume (GBMW) was used as an implicit solvation model. Interactions including hydrogen bond, electrostatic and hydrophobic effects between one ligand and two receptors of each complex were analyzed. Residues of RANKL that showed more interactions with OPG than RANK were selected to do further calculations on mutation binding energy difference. Predicted differences in RANK or OPG binding energy ($\Delta\Delta G_i$) of the RANKL mutants compared to RANKL_WT were determined through interaction energy calculation as previously described [10].

Site-directed mutagenesis, production, and purification of the RANKL variants

cDNA corresponding to mouse soluble RANKL (aa 160–316) was cloned in pET15b (Novagen, Darmstadt, Germany) using *Nco*I and *BamH*I restriction sites. Mutants were constructed by QuikChange PCR method using Phusion high-fidelity DNA polymerase (New England Biolabs, Ipswich, MA, USA). For full randomization of each residue, the small-intelligent method was used by mixing four pairs of complementary primers with degenerate codons NDT, VMA, ATG, and TGG at a ratio of 12 : 6 : 1 : 1 [39,40]. The PCR products were digested with *DpnI* (Fermentas, St. Leon, Lithuania) enzymes and then transformed into *Escherichia coli* DH5a cells. The colonies were transferred to a 96-well Luria–Bertani (LB) agar plate with 100 $\mu g \cdot mL^{-1}$ ampicillin and sequenced by GATC Biotech (Constance, Germany). After confirming the sequences of mutations, the plasmids were transformed into *E. coli* BL21(DE3) cells individually. Homotrimeric RANKL proteins were produced and purified as described before [10]. For prescreen using ELISA assay, the purities of the RANKL samples after cation exchange column (SP column, GE Healthcare, Uppsala, Sweden) were sufficient.

Prescreen ELISA

Murine RANK-Fc (R&D Systems, Minneapolis, MN, USA) and murine OPG-Fc (Bio Legends, San Diego, CA, USA) (100 μL, 10 nM) were immobilized on a 96-well high binding plate (Greiner, Frickenhausen, Germany) by in 0.1 M $NaHCO_3$ (Merck, Darmstadt, Germany) buffer pH 8.6 overnight at 4 °C, respectively. The wells were subsequently washed with PBS buffer including 0.05% v/v Tween 20 (PBST; Duchefa, Haarlem, the Netherlands), pH 7.4, and the remaining binding places were blocked with 2% w/v BSA (Roche, Mannheim, Germany) in PBS, pH 7.4 for 2 h. After washing for three times, 100 μL of 0.5 nM one-step purified RANKL_WT or mutants were added and incubated at room temperature for 1 h. After washing with TBST buffer, a 1 : 1000 dilution of goat anti-RANKL antibody (R&D Systems; Cat # BAF462, Lot # CLR0412011) was added and incubated for 1 h, and after washing, subsequently incubated with a 1 : 1000 anti-goat HRP-conjugated antibody (Millipore, Billerica, MA, USA). The signal was quantified using the One-step Turbo TMB reagent (ThermoScientific, Rockford, IL, USA) and stopped by 100 μL of 1 M sulfuric acid solution. The absorbance was measured at 450 nm. The percentage of RANKL mutants bound to RANK-Fc or OPG-Fc was measured relative to the binding of RANKL_WT.

Kinetic analysis by surface plasmon resonance

Binding experiments were determined using a Biacore 3000 system (GE Healthcare) at 25 °C. HBS-P buffer [10 mM HEPES, pH 7.4, 150 mM NaCl, 0.005% (v/v) surfactant P20; GE Healthcare] was used as a running buffer. A CM4 sensor chip (Biacore) was coated with

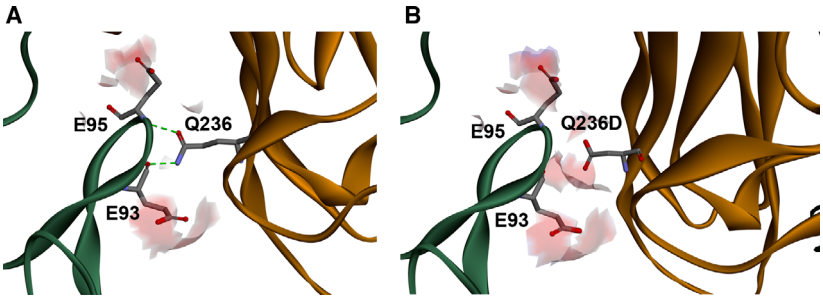

Fig. 7. Predicted area of interaction of RANKL and OPG receptor around position 236. (A) RANKL_WT and (B) RANKL_Q236D variant.

protein A (Sigma, Saint Louis, MO, USA) in 10 mM NaAc, pH 4.5. To achieve trimer–monomer complexes between ligand and receptors, RANK-Fc (Sigma) and OPG-Fc (R&D Systems) were captured at a low density, not exceeding 60 RU, with a flow rate of 50 $\mu L \cdot min^{-1}$. RANKL was injected subsequently at in concentrations between 0.01 and 160 nM for 3 min, followed by a disassociation period for 1000 s. The chip surface was regenerated by two injections of 10 mM glycine, pH 1.5–2.0 (30 s). The response data were corrected for buffer effect and was fitted to a 1 : 1 Langmuir model using the BIAEVALUATION software version 4.2 (GE Healthcare, Uppsala, Sweden).

Real-time quantitative PCR

Murine RAW 264.7 cells were a kind gift obtained from J. Doktor (University Medical Center Groningen, Groningen, the Netherlands). Cells were cultured in Dulbecco's modified Eagle's medium (Life Technologies, Carlsbad, CA, USA) with 10% v/v FBS (Life Technologies) and 2 mM penicillin/streptomycin (Life Technologies). RAW 264.7 cells were seeded at a density of 2×10^5 cells per well in a 12-well plate (Greiner) and allowed to adhere for overnight. On day 2, 50 $ng \cdot mL^{-1}$ RANKL_WT, combination of 50 $ng \cdot mL^{-1}$ RANKL_WT plus 400 $ng \cdot mL^{-1}$ mOPG-Fc (R&D) and combinations of 50 $ng \cdot mL^{-1}$ RANKL mutants plus 400 $ng \cdot mL^{-1}$ mOPG-Fc were added to the cells for 24 h.

Cells of each treatment were harvested and total mRNA was extracted using Maxwell LEX simply RNA Cells/Tissue kit (Promega, Madison, WI, USA) according to instruction described. The concentration of mRNA was measured using Nanodrop ND-100 spectrophotometer (Nanodrop Technologies, Wilmington, DE, USA). cDNA was obtained through a reverse transcription reaction using M-MLV reverse transcriptase (Promega) and random primers (Promega). The quantitative real-time PCR was performed using SensiMix™ SYBR kit (Bioline, Taunton, MA, USA) with the following specific primer sequences: GAPDH, 5′-ACAGTCCATGCCATCACTGC-3′ (forward) and 5′-GATCCACGACGGACATTG-3′ (reverse); MMP-9, 5′-GTCCAGACCAAGGGTACAGC-3′ (forward) and 5′-GCCTTGGGTCAGGCTTAGAG-3′ (reverse); TRAP, 5′-ACTTCCCCAGCCCTTACTACCG-3′ (forward) and 5′-TCAGCACATAGCCCACACCG-3′ (reverse). Thermal cycling and fluorescence detection were performed using QuantStudio real time PCR System (Thermo Fischer) and C_t values were calculated using QUANTSTUDIO REAL TIME PCR software v1.3 (Thermo Fischer, Waltham, MA, USA). For each sample, mRNA expression was normalized to GAPDH and calculated with the $2^{-\Delta\Delta C_t}$ method.

Osteoclast differentiation assay

The biological activities of RANKL_WT and mutants were evaluated using trap activity assay. RAW 264.7 cells were seeded into a 96-well plate with a density of 2500 cells per well. On day 2, cells were treated with 25 $ng \cdot mL^{-1}$ of RANKL with or without 200 $ng \cdot mL^{-1}$ of mOPG-Fc. After 4 days of treatment, cells were washed with PBS buffer and fixed with 4% fomaldehyd (Sigma) at 37 °C for 1 h. After washing with PBS buffer, the cells were then lysed for 5 min with lysis buffer containing 0.2 M Sodium acetate, 20 mM tartaric acid, and 1% triton X-100. After lysis, the plate was centrifuged for 5 min at 200 ***g*** and the supernatants were removed. The cells were then incubate with paranitrophenylphosphate (pNPP) solution containing 20 mM pNPP, 0.2 M Sodium acetate, 20 mM tartaric acid, and 30 mM potassium chloride (100 µL per well) at 37 °C for 1 h. The reaction was stopped with 1 M NaOH (100 µL per well) and the absorbance was measured at 405/410 nm using a microplate reader (Thermo Labsystems, Beverly, MA, USA). The absorbance in the wells containing 25 $ng \cdot mL^{-1}$ RANKL_WT was set to 100%.

The osteoclast differentiation assay was performed as well. As previously described [10], RAW 264.7 cells were seeded with a density of 1000 cells per well in a 96-well plate. At day 3 and day 5, cells were treated

with 50 ng·mL^{-1} of RANKL with or without 400 ng·mL^{-1} of mOPG-Fc. At day 7, osteoclast formation was determined using the TRAP staining kit (Sigma) according to the manufacturer's instructions. Multinucleated (three or more nuclei) TRAP-positive cells were treated as osteoclasts and counted under the microscope. The number of osteoclasts in the wells containing 50 ng·mL^{-1} RANKL_WT was set to 100%.

Acknowledgements

This work was performed within the framework of the Dutch Top Institute Pharma project TNF-ligands in cancer (project nr. T3-112) and STW grant 11056. YW is a recipient of a scholarship from the Chinese Scholarship Council (CSC). We thank B.N. Melgert and H. Habibie from Department of Pharmacokinetics, Toxicology and Targeting, Groningen Research Institute of Pharmacy, University of Groningen for their guidance and assistance in Real-time quantitative PCR measurement and TRAP activity assay.

Conflict of interest

The authors declare no conflict of interest.

Author contributions

YW, TM, RS, RM, and RHC performed experiments and analyzed data; WJQ planned the research and supervised the study; YW and WJQ wrote the paper.

References

1 Trouvin AP & Goëb V (2010) Receptor activator of nuclear factor-κB ligand and osteoprotegerin: maintaining the balance to prevent bone loss. *Clin Interv Aging* **5**, 345–354.
2 Naidu VGM, Dinesh Babu KR, Thwin MM, Satish RL, Kumar PV & Gopalakrishnakone P (2013) RANKL targeted peptides inhibit osteoclastogenesis and attenuate adjuvant induced arthritis by inhibiting NF-κB activation and down regulating inflammatory cytokines. *Chem Biol Interact* **203**, 467–479.
3 Douni E, Rinotas V, Makrinou E, Zwerina J, Penninger JM, Eliopoulos E, Schett G & Kollias G (2012) A RANKL G278R mutation causing osteopetrosis identifies a functional amino acid essential for trimer assembly in RANKL and TNF. *Hum Mol Genet* **21**, 784–798.
4 Lam J, Nelson CA, Ross FP, Teitelbaum SL & Fremont DH (2001) Crystal structure of the RANCE/RANKL cytokine reveals determinants of receptor ligand specificity. *J Clin Invest* **108**, 971–979.
5 Ito S, Wakabayashi K, Ubukata O, Hayashi S, Okada F & Hata T (2002) Crystal structure of the extracellular domain of mouse RANK ligand at 2.2-Å resolution. *J Biol Chem* **277**, 6631–6636.
6 Chaweewannakorn W, Ariyoshi W, Okinaga T, Fujita Y, Maki K & Nishihara T (2019) Ameloblastin attenuates RANKL-mediated osteoclastogenesis by suppressing activation of nuclear factor of activated T-cell cytoplasmic 1 (NFATc1). *J Cell Physiol* **234**, 1745–1757.
7 Rachner TD, Khosla S & Hofbauer LC (2011) Osteoporosis: now and the future. *Lancet* **377**, 1276–1287.
8 Holen I & Shipman CM (2006) Role of osteoprotegerin (OPG) in cancer. *Clin Sci* **110**, 279–291.
9 Ta HM, Nguyen GTT, Jin HM, Choi J, Park H, Kim N, Hwang H-Y & Kim KK (2010) Structure-based development of a receptor activator of nuclear factor-B ligand (RANKL) inhibitor peptide and molecular basis for osteopetrosis. *Proc Natl Acad Sci USA* **107**, 20281–20286.
10 Wang Y, van Assen AHG, Reis CR, Setroikromo R, van Merkerk R, Boersma YL, Cool RH & Quax WJ (2017) Novel RANKL DE-loop mutants antagonize RANK-mediated osteoclastogenesis. *FEBS J* **284**, 2501–2512.
11 Liu C, Walter TS, Huang P, Zhang S, Zhu X, Wu Y, Wedderburn LR, Tang P, Owens RJ, Stuart DI *et al.* (2010) Structural and functional insights of RANKL-RANK interaction and signaling. *J Immunol* **184**, 6910–6919.
12 Szalay F, Hegedus D, Lakatos PL, Tornai I, Bajnok E, Dunkel K & Lakatos P (2003) High serum osteoprotegerin and low RANKL in primary biliary cirrhosis. *J Hepatol* **38**, 395–400.
13 Todd NW, Luzina IG & Atamas SP (2012) Molecular and cellular mechanisms of pulmonary fibrosis. *Fibrogenesis Tissue Repair* **5**, 11.
14 Murtha LA, Schuliga MJ, Mabotuwana NS, Hardy SA, Waters DW, Burgess JK, Knight DA & Boyle AJ (2017) The processes and mechanisms of cardiac and pulmonary fibrosis. *Front Physiol* **8**, 1–15.
15 Wynn TA (2011) Integrating mechanisms of pulmonary fibrosis. *J Exp Med* **208**, 1339–1350.
16 Raghu G & Richeldi L (2017) Current approaches to the management of idiopathic pulmonary fibrosis. *Respir Med* **129**, 24–30.
17 Florez-Sampedro L, Song S & Melgert BN (2018) The diversity of myeloid immune cells shaping wound repair and fibrosis in the lung. *Regeneration* **5**, 3–25.
18 Beljaars L, Schippers M, Reker-Smit C, Martinez FO, Helming L, Poelstra K & Melgert BN (2014) Hepatic localization of macrophage phenotypes during

fibrogenesis and resolution of fibrosis in mice and humans. *Front Immunol* **5**, 430.
19 Boorsma CE, Draijer C & Melgert BN (2013) Macrophage heterogeneity in respiratory diseases. *Mediators Inflamm* **2013**, 769214.
20 Adhyatmika A, Putri KSS, Beljaars L & Melgert BN (2015) The elusive antifibrotic macrophage. *Front Med* **2**, 1–11.
21 Tosi P (2013) Diagnosis and treatment of bone disease in multiple myeloma: spotlight on spinal involvement. *Scientifica (Cairo)* **2013**, 1–12.
22 Okamoto K, Nakashima T, Shinohara M, Negishi-Koga T, Komatsu N, Terashima A, Sawa S, Nitta T & Takayanagi H (2017) Osteoimmunology: the conceptual framework unifying the immune and skeletal systems. *Physiol Rev* **97**, 1295–1349.
23 Toffoli B, Pickering RJ, Tsorotes D, Wang B, Bernardi S, Kantharidis P, Fabris B, Zauli G, Secchiero P & Thomas MC (2011) Osteoprotegerin promotes vascular fibrosis via a TGF-β1 autocrine loop. *Atherosclerosis* **218**, 61–68.
24 Ambroszkiewicz J, Sands D, Gajewska J, Chelchowska M & Laskowska-Klita T (2013) Bone turnover markers, osteoprotegerin and RANKL cytokines in children with cystic fibrosis. *Adv Med Sci* **58**, 338–343.
25 García-Valdecasas-Campelo E, González-Reimers E, Santolaria-Fernández F, De la Vega-Prieto MJ, Milena-Abril A, Sánchez-Pérez MJ, Martínez-Riera A & De Los Ángeles Gómez-Rodríguez M (2006) Serum osteoprotegerin and rankl levels in chronic alcoholic liver disease. *Alcohol Alcohol* **41**, 261–266.
26 Reis CR, van Assen AHG, Quax WJ & Cool RH (2011) Unraveling the binding mechanism of trivalent tumor necrosis factor ligands and their receptors. *Mol Cell Proteomics* **10**, M110.002808.
27 Eriksen EF (2010) Cellular mechanisms of bone remodeling. *Rev Endocr Metab Disord* **11**, 219–227.
28 Kim J & Kim N (2016) Signaling pathways in osteoclast differentiation. *Chonnam Med J* **52**, 12–17.
29 Feng W, Li W, Liu W, Wang F, Li Y & Yan W (2009) IL-17 induces myocardial fibrosis and enhances RANKL/OPG and MMP/TIMP signaling in isoproterenol-induced heart failure. *Exp Mol Pathol* **87**, 212–218.
30 Renema N, Navet B, Heymann M-F, Lezot F & Heymann D (2016) RANK-RANKL signalling in cancer. *Biosci Rep* **36**, e00366.
31 Bosman MCJ, Reis CR, Schuringa JJ, Vellenga E & Quax WJ (2014) Decreased affinity of recombinant human tumor necrosis factor-related apoptosis-inducing ligand (rhTRAIL) D269H/E195R to osteoprotegerin (OPG) overcomes trail resistance mediated by the bone microenvironment. *J Biol Chem* **289**, 1071–1078.
32 Van der Sloot AM, Tur V, Szegezdi E, Mullally MM, Cool RH, Samali A, Serrano L & Quax WJ (2006) Designed tumor necrosis factor-related apoptosis-inducing ligand variants initiating apoptosis exclusively via the DR5 receptor. *Proc Natl Acad Sci USA* **103**, 8634–8639.
33 Nelson CA, Warren JT, Wang MWH, Teitelbaum SL & Fremont DH (2013) RANKL employs distinct binding modes to engage RANK and the OPG decoy receptor Christopher. *Structure* **20**, 1971–1982.
34 Luan X, Lu Q, Jiang Y, Zhang S, Wang Q, Yuan H, Zhao W, Wang J & Wang X (2016) Crystal structure of human RANKL complexed with its decoy receptor opsteoprotegerin. *J Immunol* **189**, 245–252.
35 Tur V, Van der Sloot AM, Reis CR, Szegezdi E, Cool RH, Samali A, Serrano L & Quax WJ (2008) DR4-selective tumor necrosis factor-related apoptosis-inducing ligand (TRAIL) variants obtained by structure-based design. *J Biol Chem* **283**, 20560–20568.
36 Warren JT, Zou W, Decker CE, Rohatgi N, Nelson CA, Fremont DH & Teitelbaum SL (2015) Correlating RANK ligand/RANK binding kinetics with osteoclast formation and function. *J Cell Biochem* **116**, 2476–2483.
37 Rockey DC, Bell PD & Hill JA (2015) Fibrosis – a common pathway to organ injury and failure. *N Engl J Med* **372**, 1138–1149.
38 Said A & Lucey MR (2008) Liver transplantation: an update 2008. *Curr Opin Gastroenterol* **24**, 339–345.
39 Tang L, Gao H, Zhu X, Wang X, Zhou M & Jiang R (2012) Construction of "small-intelligent" focused mutagenesis libraries using well-designed combinatorial degenerate primers. *Biotechniques* **52**, 149–158.
40 Abdallah II, Van Merkerk R, Klumpenaar E & Quax WJ (2018) Catalysis of amorpha-4,11-diene synthase unraveled and improved by mutability landscape guided engineering. *Sci Rep* **8**, 1–11.